



# Kinetic analysis of 4,6-dimethyldibenzothiophene hydrodesulfurization in the presence of nitrogen compounds

Matheus da Silva Campos Machado<sup>1,\*</sup>, Idia Gigante Nascimento<sup>1</sup>, Matheus Dorneles de Mello<sup>2</sup>, Mônica Antunes Pereira da Silva<sup>1</sup>

<sup>1</sup>Escola de Química/Universidade Federal do Rio de Janeiro, Rio de Janeiro, Brazil

<sup>2</sup>Dow Chemicals, Michigan, United States of America

\*E-mail: matheuscampos@eq.ufrj.br

## Resumo/Abstract

RESUMO – A limitação do teor de enxofre em combustíveis, especialmente no diesel, é uma exigência ambiental crescente. Para atendê-la, as refinarias empregam a hidrodessulfurização profunda (HDS). Esse processo catalítico, que opera sob condições de média severidade, é necessário para a remoção dos compostos sulfurados mais refratários, como o 4,6-dimetildibenzotiofeno (4,6-DMDBT), além de inibidores, como os compostos nitrogenados. Nesse contexto, este trabalho propôs um modelo cinético de Langmuir-Hinshelwood para descrever as reações simultâneas de HDS do 4,6-DMDBT e hidrodesnitrogenação da quinolina, considerando que compostos nitrogenados inibem a HDS e exigem condições operacionais mais severas. Os experimentos foram conduzidos em reator de leito fixo, utilizando NiMoP/ $\gamma$ -Al<sub>2</sub>O<sub>3</sub> como catalisador. O modelo cinético apresentou um bom ajuste, com coeficiente de determinação (R<sup>2</sup>) de 0,93 entre os valores experimentais e simulados. A energia de ativação para a rota de hidrogenação prévia do 4,6-DMDBT foi estimada em 259,3  $\pm$  16,0 kJ mol<sup>-1</sup>. Esse valor é superior ao obtido para a rota de dessulfurização direta (191,7  $\pm$  10,7 kJ mol<sup>-1</sup>), um comportamento não observado na literatura na ausência de compostos nitrogenados.

Palavras-chave: Hidrodessulfurização, hidrodesnitrogenação, 4,6-dimetildibenzotiofeno, NiMo, Langmuir-Hinshelwood

ABSTRACT – The limitation of sulfur content in fuels, particularly diesel, has become an increasingly stringent environmental requirement. To comply with this regulation, refineries employ deep hydrodesulfurization (HDS). This catalytic process, which operates under moderately severe conditions, is essential for the removal of more refractory sulfur compounds, such as 4,6-dimethyldibenzothiophene (4,6-DMDBT), as well as nitrogen-containing inhibitors. In this context, the present study proposes a Langmuir-Hinshelwood kinetic model to describe the simultaneous reactions of HDS of 4,6-DMDBT and hydrodenitrogenation of quinoline, considering that nitrogen-containing compounds inhibit HDS and necessitate more severe operating conditions. Experiments were conducted in a fixed-bed reactor using NiMoP/ $\gamma$ -Al<sub>2</sub>O<sub>3</sub> as the catalyst. The kinetic model exhibited a good fit with the experimental data, presenting a coefficient of determination (R<sup>2</sup>) of 0.93 between the experimental and simulated values. The activation energy for the prior hydrogenation route of 4,6-DMDBT was estimated to be 259.3 ± 16.0 kJ mol<sup>-1</sup>. This value is higher than the one obtained for the direct desulfurization route (191.7 ± 10.7 kJ mol<sup>-1</sup>), a behavior not reported in the literature for systems in the absence of nitrogenous compounds.

Keywords: Hydrodesulfurization, hydrodenitrogenation, 4,6-dimethyldibenzothiophene, NiMo, Langmuir-Hinshelwood

# Introduction

A regulatory measure implemented by governments worldwide to mitigate climate change involves restricting the maximum sulfur content in fuels to below 10-15 mg kg<sup>-1</sup>. To comply with this specification, refineries implement deep hydrodesulfurization (HDS), a catalytic process that uses hydrogen under moderately severe conditions (T = 340 °C and P = 100 bar) to remove refractory sulfur components and inhibitors (1, 2). Moreover, the hydrogen used in HDS is primarily produced via steam methane reforming (SMR), one of the major sources of  $CO_2$  emissions in the refining process. Therefore,

reducing unnecessary hydrogen consumption through kinetic investigations is essential to enhance both environmental sustainability and economic performance (3)

HDS is typically inhibited by hydrodenitrogenation (HDN) due to the strong adsorption of nitrogen-containing compounds on the catalyst's active sites (4). Among transportation fuels, diesel is the most widely used for heavy-duty trucks worldwide, owing to its high energy density (5). To enable kinetic studies, model molecules are commonly employed to simulate real fuels. In the case of HDS, 4,6-dimethyldibenzothiophene (4,6-DMDBT) is



used, as it is one of the most refractory sulfur compounds present in significant quantities in diesel (3, 6).

The HDS of 4,6-DMDBT proceeds via two main pathways, as illustrated in Figure 1. The first is the hydrogenation (HYD) route, which involves the formation of partially hydrogenated intermediates prior to C-S bond cleavage, yielding methylcyclohexyltoluene (MCHT). Further hydrogenation of MCHT can lead to the formation of dimethyldicyclohexane (DMDCH). The second pathway is direct desulfurization (DDS), characterized by the direct cleavage of the C-S bond at hydrogenolysis sites, resulting in the formation of 3,3'-dimethylbiphenyl (3,3'-DMBP). 4,6-DMDBT preferentially reacts via the HYD route due to its high stability, which arises from the presence of aromatic rings and two methyl groups in its structure, both of which hinder the access of sulfur to the catalyst's active sites (7).

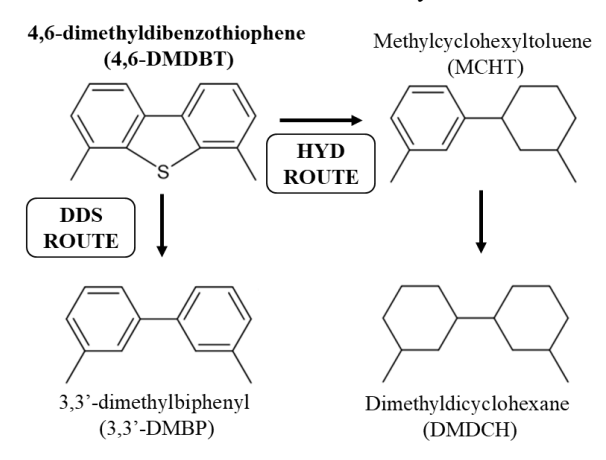


Figure 1. HDS pathways of 4,6-DMDBT.

For HDN, quinoline (Q) is commonly employed as a model compound, since it undergoes all the steps involved in HDN mechanism, as shown in Figure 2 (8).

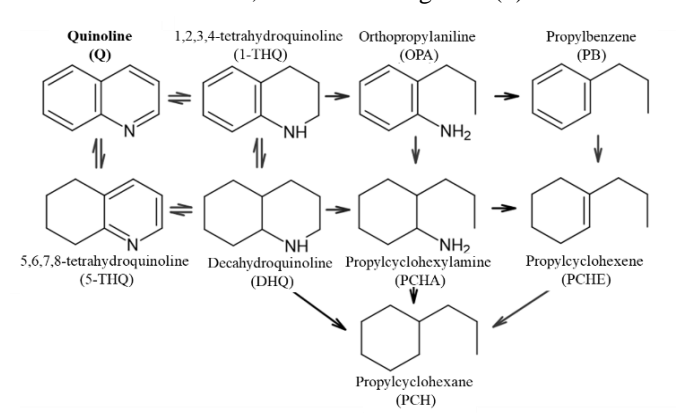


Figure 2. HDN pathways of quinoline.

Industrial HDS catalysts typically consist of molybdenum or tungsten sulfides, promoted by nickel or cobalt, and supported on alumina. Nickel promotion enhances hydrogenation activity, whereas cobalt promotion favors hydrogenolysis sites (9).



Therefore, this study aims to evaluate the kinetics of simultaneous HDS of 4,6-DMDBT and HDN of quinoline based on a Langmuir-Hinshelwood (LH) model, employing a NiMoP/ $\gamma$ -Al<sub>2</sub>O<sub>3</sub> catalyst in a fixed bed reactor operating in continuous mode.

# Experimental

Catalyst preparation and characterization

NiMoP/γ-Al<sub>2</sub>O<sub>3</sub> was synthesized using the incipient wetness impregnation method, as described by Nascimento et al. (10). The catalyst formulation consisted of 20 % (m/m) of MoO<sub>3</sub>, with atomic ratios of 0.3 for and 0.4 P/Mo. Ni/(Ni + Mo)for Ammonium heptamolybdate (99 % - VETEC), nickel nitrate (97 % - VETEC) and phosphoric acid (85 % - VETEC) were used as metal precursors, with Pural SB alumina employed as the support. The oxide form of the catalyst was characterized by Nascimento et al. (10) using inductively coupled plasma optical emission spectrometry (ICP-OES), X-ray diffraction (XRD), nitrogen physisorption, and thermogravimetric analysis (TGA). Additionally, Guedes Júnior et al. (11) investigated the sulfided form using X-ray photoelectron spectroscopy (XPS) and high-resolution transmission electron microscopy (HRTEM).

# Catalyst Activation

Following reactor loading, the catalyst was activated *in situ* via sulfidation, using a solution containing 4 % (w/w) carbon disulfide (CS<sub>2</sub>, PA – VETEC) dissolved in *n*-hexane (97 % - VETEC). The procedure was carried out under 30 bar of  $H_2$ , with a weight hourly space velocity (WHSV) of 4  $h^{-1}$ , and two temperature stages: the first at 250 °C for 2 h, followed by 350 °C for 3 h, with a heating rate of 2 °C min<sup>-1</sup>.

## Reaction system

Experiments were conducted in an up-flow flooded-bed reactor (PID Eng & Tech). The feed consisted of n-hexadecane (99 % - Sigma) containing 1000 mg kg<sup>-1</sup> of sulfur from 4,6-DMDBT (95 % - BOC Sciences) and 150-250 mg kg<sup>-1</sup> of nitrogen from quinoline (96 % - Acros Organic). A catalyst mass used was 1.14 g, with particle sizes in the range of 0.090 mm to 0.125 mm. The operating conditions included temperatures between 310 and 340 °C, WHSV from 8 to 14 h<sup>-1</sup> and H<sub>2</sub> pressure ranging from 30 to 60 bar, resulting in a total of 13 experiments. The H<sub>2</sub>/feed ratio was maintained constant at 400 NL L<sup>-1</sup>. The concentration of dissolved H2 in the liquid phase was determined using HYSYS software, applying the Soave-Redlich-Kwong (SRK) equation of state. Liquid samples were periodically collected until steady-state was achieved, defined by a conversion relative error below 2 %, normally reached after 7 hours of reaction. Samples were analyzed by



gas chromatography (Agilent 7820A) equipped with a flame ionization detection (FID) and DB-1 capillary column (60 m x 0.32 mm x 0.5  $\mu$ m thickness).

## Estimation of kinetic parameters

To minimize the objective function  $(F_{obj})$  based on a weighted least squares criterion, a hybrid optimization approach was employed by integrating the heuristic method of particle swarm optimization (PSO) with the deterministic Gauss-Newton method. PSO was applied to identify the global minimum, using a swarm of 100 particles over 1000 iterations. The individual and group contribution to particle speed were both set to 1.5, and the factor of inertia was fixed at 0.75. A step tolerance of 10<sup>-10</sup> was adopted, and the convergence criterion for the objective function was set to 10<sup>-8</sup>. To reduce the parametric correlation between the activation energy and the pre-exponential factor, the Arrhenius equation was reparameterized using an optimized reference temperature, as presented in Equations 1-3. Model performance was evaluated using the coefficient of determination (R<sup>2</sup>), the chi-square ( $\chi^2$ ) test, and the confidence intervals of the estimated parameters, which were calculated using the t-Student distribution at a 95 % confidence level.

$$k_{j} = \exp\left(-a_{i} + b_{i}\left(1 - \frac{T_{ref,j}}{T}\right)\right) \tag{1}$$

$$E_j = R T_{ref,i} b_i (2)$$

$$ln k_{0,i} = \exp(b_i - a_i)$$
(3)

where,  $a_i$  and  $b_i$  are estimated model parameters;  $k_j$  and  $k_{0,j}$  represent the specific rate constant and the corresponding pre-exponential factor for reaction j, respectively;  $k_{0,j}$  and  $T_{ref,j}$  denote the temperature and reference temperature for reaction j, respectively; R is the universal gas constant; and  $E_j$  is the activation energy for reaction j.

The variance  $(\sigma^2)$  used in the parameter estimation was calculated according to Equation (4):

$$\sigma^2 = \frac{\sum (c - \bar{c})^2}{n - 1} \tag{4}$$

where c and  $\bar{c}$  are molar concentration (mol L<sup>-1</sup>) and average molar concentration (mol L<sup>-1</sup>), respectively.

# Results and Discussion

# Characterizations

ICP analysis of the catalyst in its oxide form, as reported by Nascimento *et al.* (10), confirmed that the metal loading was consistent with the nominal formulation. XRD and nitrogen physisorption measurements indicated that the structural and textural properties of the support were preserved after impregnation. Furthermore, TGA results



validated the calcination temperature employed during catalyst preparation.

In the sulfided form, Guedes *et al.* (11) observed via XPS that the most of the Mo species were present as sulfides. However, a notable presence of Mo and Ni in oxide forms was also detected, which was attributed to possible oxidation during sample handling and transportation. HRTEM analysis further revealed approximately 30 % dispersion of Ni within the  $MoS_2$  slabs.

#### Kinetic model

Figure 3 shows the reaction scheme adopted for the kinetic modeling. In this scheme, 4,6-DMDBT proceeds via two parallel pathways: DDS route, in which hydrogen concentration is assumed constant due to its negligible effect on model fitting, and HYD route, represented by the formation of MCHT and DMBCH. The intermediate step involving the conversion of MCHT to DMBCH was excluded from the model, as the associated estimated parameters exhibited uncertainties greater than their respective values. The HDN pathway is simplified by representing the conversion of nitrogen-containing compounds (N) directly into non-nitrogenated products (NN).

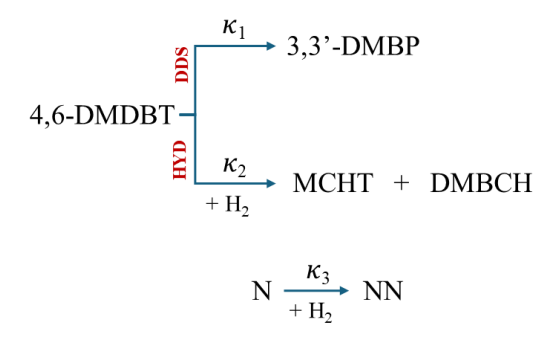


**Figure 3.** Schematic representation of the proposed reaction network.

Equations 5-10 used in the modeling were simplified by assuming an ideal reactor (isothermal, isobaric and one-dimensional direction) operating under steady-state. Diffusional limitations were considered negligible, as verified by the Weisz and Prater (12), and Mears criteria (13). Consequently, the reaction rate was governed by surface kinetics. The Langmuir-Hinshelwood model was employed, assuming a single type of active site, non-dissociative hydrogen adsorption and competitive adsorption limited to nitrogenous compounds. To simplify the kinetic model, all constants, including the total active sites, intrinsic kinetic constants, and reagent adsorption constants, were grouped into a single lumped parameter, denoted as  $\kappa$ . An empirical exponent ( $\delta$ ) was introduced to improve the model's accuracy, with a value of  $\delta = 1.5$ , as reported in the literature (14, 15). Additionally, the



adsorption equilibrium constant of nitrogenous compounds  $(K_N)$  was taken from the expression reported by Nguyen *et al.* (8).

$$\frac{dC_{4,6DMDBT}}{d\tau} = -\frac{\rho \kappa_1 C_{4,6DMDBT}}{1 + K_N^{\delta} C_N^{\delta}} - \frac{\rho \kappa_2 C_{4,6DMDBT} C_{H_2}}{1 + K_N^{\delta} C_N^{\delta}}$$
(5)

$$\frac{dC_{3,3DMBP}}{d\tau} = \frac{\rho \kappa_1 C_{4,6DMDBT}}{1 + K_N^{\delta} C_N^{\delta}} \tag{6}$$

$$\frac{dC_{MCHT}}{d\tau} = \frac{\rho \kappa_2 C_{4,6DMDBT} C_{H_2}}{1 + K_N^{\delta} C_N^{\delta}}$$
 (7)

$$\frac{dC_N}{d\tau} = -\frac{\rho \kappa_3 C_N C_{H_2}}{1 + K_N^{\delta} C_N^{\delta}} \tag{8}$$

$$\frac{dC_{NN}}{d\tau} = \frac{\rho \kappa_3 C_N C_{H_2}}{1 + K_N^{\delta} C_N^{\delta}} \tag{9}$$

$$K_N = 5.45 \times 10^{-7} \exp\left(\frac{48200}{RT}\right) \tag{10}$$

where,  $C_i$  is the molar concentration of compound i (mol L<sup>-1</sup>);  $\tau$  is the space time (h);  $\rho$  is the fluid mass density (kg L<sup>-1</sup>); and  $K_N$  is the adsorption equilibrium constant of nitrogenous compounds (L mol<sup>-1</sup>).

The parameter estimates and results of objective function are presented in Tables 1 and 2, respectively.

Table 1: Parameter estimates for HDS and HDN reactions.

| The 1. I arameter estimates for Tids and Tidin feaction   |                  |  |  |
|---|------------------|--|--|
| Estimated parameters  |                  |  |  |
| $a_1$   | $-1.27 \pm 0.04$ |  |  |
| $b_1$   | $38.9 \pm 2.2$   |  |  |
| $a_2$   | $-3.03 \pm 0.07$ |  |  |
| $b_2$   | $52.2 \pm 3.2$   |  |  |
| $a_3$   | $-4.00 \pm 0.08$ |  |  |
| $b_3$   | $38.3 \pm 7.4$   |  |  |
| Kinetic parameters  |                  |  |  |
| $\ln (\kappa_1^0)$  | $40.1 \pm 2.2$   |  |  |
| $E_1$ (kJ mol <sup>-1</sup> )   | $191.7 \pm 10.7$ |  |  |
| $\ln (\kappa_2^0)$  | $55.2 \pm 3.2$   |  |  |
| $E_2$ (kJ mol <sup>-1</sup> )   | $259.3 \pm 16.0$ |  |  |
| $\ln (\kappa_3^0)$  | $42.3 \pm 7.4$   |  |  |
| $E_3$ (kJ mol <sup>-1</sup> )   | $186.8 \pm 36.0$ |  |  |
| $T_{ref1} = 320  ^{\circ}\text{C},  T_{ref2} = 325  ^{\circ}\text{C}  \text{and}  T_{ref3} = 313  ^{\circ}\text{C}$ |                  |  |  |

Table 2: Objective function results.

| $\chi^2_{min}$ | $F_{obj}$ | $\chi^2_{max}$ | $R^2$ |
|----------------|-----------|----------------|-------|
| 40             | 357       | 82             | 0.93  |

All parameters were found to be statistically significant according to the *t*-Student test.

Although the value of objective function exceeds the chi-square maximum limit, suggesting that the experimental errors may have been underestimated. Nevertheless, the model still exhibited strong predictive performance, with a



coefficient of determination ( $R^2$ ) greater than 0.9, indicating a good fit to the experimental data, as shown in Figure 4.

The estimated activation energies for HDS were  $191.7 \pm 10.7 \text{ kJ mol}^{-1}$  for the DDS route and  $259.3 \pm 16.0 \text{ kJ mol}^{-1}$  for the HYD route. For the HDN reaction, an activation energy of  $186.8 \pm 35.9 \text{ kJ mol}^{-1}$  was obtained. Compared to literature values reported in the absence of inhibitory species (13, 16), an inversion of the preferential HDS pathway was observed in the presence of quinoline. This inversion is evidenced by the higher activation energy associated with the HYD route, suggesting that the inhibitory effect of nitrogen-containing compounds is more significant than the steric hindrance caused by the methyl substituents.

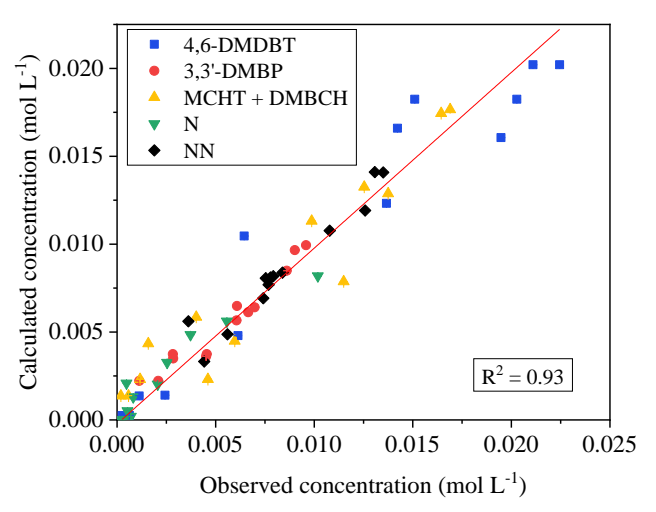


**Figure 4.** Fit of the experimental data using the Langmuir-Hinshelwood model.

## Conclusions

A Langmuir-Hinshelwood kinetic model was developed to describe the simultaneous hydrodesulfurization and hydrodenitrogenation reactions carried out in a flooded-bed reactor using a NiMoP/ $\gamma$ -Al<sub>2</sub>O<sub>3</sub> catalyst. The kinetic parameters were successfully estimated, demonstrating the model's consistency with the experimental data. Additionally, the activation energy associated with the DDS pathway was lower than that of the HYD route, which it is not observed in the absence of nitrogen-containing compounds. This finding suggests that the presence of such compounds can significantly influence the reaction network modifying the preferred reaction pathway of 4,6-DMDBT.

## Acknowledgments

The authors thank for financial support: ANP (Agência Nacional de Petróleo) and FAPESP (Fundação de Amparo à Pesquisa do Estado de São Paulo) via Programa de Recursos Humanos da ANP para o Setor de Petróleo, Gás Natural e Biocombustíveis (PRH-ANP), in particular PRH 3.1 – EQ-PEQ-COPPE/UFRJ; CAPES (Coordenação de Aperfeiçoamento de Pessoal de Nível Superior - Brasil)





- Finance Code 001; Conselho Nacional de Desenvolvimento Científico e Tecnológico (CNPq), Grant No. 307190/2022-6, and Fundação Carlos Chagas Filho de Amparo à Pesquisa do Estado do Rio de Janeiro (FAPERJ), Grant No. E-26/211.578/2021.

## References

- W. Han; Y. Gao; S. Zhou; X. Long; J. Liu; H. Nie, Sep. Purif. Technol. 2025, 359, 130685.
- D. Chehadeh; X. Ma; H. Bazzaz, Fuel. 2023, 334, 126404.
- Y. Zhang; F. Liu; W. Chen; W. Han; W. Zhai; Y. Lu;
   M. Li, Fuel. 2024, 356, 129640.
- 4. Y. Yin; W. Chen; G. Wu; F. Xin; K. Qin; Y. Lu; L. Zhang; M. Li, *Aiche J.* **2020**, *67*, 1-14.
- A. C. R. Texeira; P. G. Machado; F. M. A. Collaço; D. Mouette, *Environ. Sci. Pollut. Res.* 2021, 28, 20954-20969.
- L. Gao; W. He; W. Zhai; M. Xin; W. Wang; Y. Xiang;
   H. Yuan; S. Wang; F. Liu; G. Xu; L. Qiu; M. Li, Fuel.
   2025, 393, 135052.
- Q. Li; Z. Xiao; H. Xin; G. Li; D. Wang; C. Feng; X. Li;
   S. Chen; K. H. Chung, *Chem. Eng. J.* 2023, 472, 145128.
- 8. M. T. Nguyen; M. Tayakout-Fayolle; G. D. Pirngruber; F. Chainet; C. Geantet, *Ind. Eng. Chem. Res.* **2015**, *54*, 9278–9288.
- W. Huang; Q. Wei; Y. Zhou; X. Liu; M. Liu; P. Zhang;
   Z. Xu; Z. Yu; X. Wang; H. Liu, Catal. Today. 2023, 407, 135-145.
- I. G. Nascimento; W. R. Locatel; B. C. Magalhães; L. Travalloni; J. L. Zotin; M. A. P. Silva, *Catal. Today*. 2021, 381, 200-208.
- G. S. Guedes Júnior; I. G. Nascimento; M. Ahmad; C. Killeen; J. A. Bascoboinik; J. Trelewicz; J. C. Pinto; M. D. Mello; M. A. P. Silva, *Chem. Eng. Sci.* 2023, 275, 118725.
- 12. P. B. Weisz; C. D. Prater. Adv. Catal. 1954, 6, 143–196.
- 13. D. E. Mears. Chem. Eng. Sci, 1971, 26, 1361–1366.
- M. D. Mello; F. A. Braggio; B. C. Magalhães; J. L. Zotin; M. A. P. Silva, Fuel Process. Technol. 2018, 177, 66-74.
- 15. J. C. García-Martínez; C. O. Castillo-Araiza; J. A. L. R. Heredia; E. Trejo; A. Montesinos, *Chem. Eng. J.* **2012**, *210*, 53-62.
- 16. J. H. Kim; X. Ma; C. Song; Y. Lee; S. T. Oyama, *Energy & Fuels.* **2005**, *19*, 353-364.